environmental microbiology

Environmental Microbiology (2020) **00**(00), 00–00 doi:10.1111/1462-2920.15250

Variation at the common polysaccharide antigen locus drives lipopolysaccharide diversity within the *Pseudomonas syringae* species complex

Jay Jayaraman,[1,2] William T. Jones,[3] Dawn Harvey,[3] Lauren M. Hemara,[1,2,4] Honour C. McCann,[5,†] Minsoo Yoon,[1] Suzanne L. Warring,[6] Peter C. Fineran,[2,6] Carl H. Mesarich[2,7] and Matthew D. Templeton [1,2,4*]

[1]*Bioprotection Technologies, The New Zealand Institute for Plant and Food Research Limited, Auckland, New Zealand.*

[2]*Bioprotection Centre for Research Excellence, New Zealand.*

[3]*Bioprotection Technologies, The New Zealand Institute for Plant and Food Research Limited, Palmerston North, New Zealand.*

[4]*School of Biological Sciences, University of Auckland, New Zealand.*

[5]*Institute of Advanced Studies, Massey University, Auckland, New Zealand.*

[6]*Department of Microbiology and Immunology, University of Otago, Dunedin, New Zealand.*

[7]*School of Agriculture and Environment, Massey University, Palmerston North, New Zealand.*

Summary

The common polysaccharide antigen (CPA) of the lipopolysaccharide (LPS) from *Pseudomonas syringae* is highly variable, but the genetic basis for this is poorly understood. We have characterized the CPA locus from *P. syringae* pv. *actinidiae* (*Psa*). This locus has genes for L- and D-rhamnose biosynthesis and an operon coding for ABC transporter subunits, a bifunctional glycosyltransferase and an O-methyltransferase. This operon is predicted to have a role in the transport, elongation and termination of the CPA oligosaccharide and is referred to as the TET operon. Two alleles of the TET operon were present in different biovars (BV) of *Psa* and lineages of the closely related pathovar *P. syringae* pv. *actinidifoliorum*. This allelic variation was reflected in the electrophoretic properties of purified LPS from the different isolates. Gene knockout of the TET operon allele from BV1 and replacement with that from BV3, demonstrated the link between the genetic locus and the biochemical properties of the LPS molecules in *Psa*. Sequence analysis of the TET operon from a range of *P. syringae* and *P. viridiflava* isolates displayed a phylogenetic history incongruent with core gene phylogeny but correlates with previously reported tailocin sensitivity, suggesting a functional relationship between LPS structure and tailocin susceptibility.

Received 29 April, 2020; revised 22 September, 2020; accepted 22 September, 2020. *For correspondence. E-mail matt.templeton@plantandfood.co.nz; Tel. +64-9-9257155; Fax +64-9-9257001.
†Present address: Max Planck Institute for Developmental Biology, Max-Planck-Ring 9, Tübingen, D-72076, Germany.

Introduction

Pseudomonas syringae pv. *actinidiae* (*Psa*) is the causal agent of canker disease in kiwifruit (*Actinidia* Lindl spp.). Outbreaks of the disease were first observed in Japan and Korea in the 1980s and 1990s respectively, but isolates of the bacterium responsible for these outbreaks did not spread from their country of origin (Koh *et al*., 1994; Serizawa *et al*., 1989; Takikawa *et al*., 1989). Between 2008 and 2010, a pandemic clone spread around the world, devastating the majority of regions growing cultivars of *A. chinensis* var. *chinensis* (gold kiwifruit) (Scortichini *et al*., 2012). A large number of *Psa* isolates from a range of geographical origins have been sequenced, and phylogenies generated from the core genomes show that the three emergences of the disease are closely related, but form distinct clades (McCann *et al*., 2013; McCann *et al*., 2017). Single nucleotide polymorphism (SNP) analysis indicates that the recent pandemic isolate originated in China, but the location of the source population of this pathovar has not been identified (McCann *et al*., 2017). Despite the close phylogenetic relationship between *Psa* isolates, their accessory genomes vary significantly in their effector complement and secondary metabolite portfolios (Marcelletti *et al*., 2011; Mazzaglia *et al*., 2012; Butler *et al*., 2013; McCann *et al*., 2013).

Based on both the phylogeny of the core genome and accessory gene variation, *Psa* isolates have been designated as biovars (BVs) (Vanneste *et al*., 2013; Cunty *et al*., 2015). The isolates that only cause leaf spots on kiwifruit, initially described as BV4, are closely related to *Psa*, but have now been given their own pathovar designation; *P. syringae* pv. *actinidifoliorum* (*Pfm*) and consist of four distinct lineages (L1-4; Cunty *et al*., 2015). Recently, two more *Psa* BVs have been discovered in Japan (Fujikawa and Sawada, 2016; Sawada *et al*., 2016). Variation in the accessory genome of *P. syringae* pathovars and *Psa* BVs, and its role in host specificity has been well documented (McCann *et al*., 2013; Dillon *et al*., 2019a). In addition, *P. syringae* isolates have been shown to have a high degree of structural and serological variation in their lipopolysaccharide (LPS) (Zdorovenko and Zdorovenko, 2010). However, the genetic basis for this is not well understood.

Most bacteriophages and tailocins utilize LPS as a receptor to recognize and bind to their host. Tailocins are derivatives of bacteriophages, comprising predominantly the tail proteins that function to depolarize the bacterial membrane (Riley and Wertz, 2002). It is thought that isolates of *P. syringae* use tailocins (also known as R-type syringacins) to target and outcompete closely related strains that presumably occupy a similar ecological niche (Hockett *et al*., 2015). It has been shown recently that there is a high degree of variation in the sensitivity to tailocins within *P. syringae* (Baltrus *et al*., 2019). Understanding the molecular basis of this variation is important if we are to implement novel methods such as the use of phage therapy or tailocins for biological control of this pathogen (Frampton *et al*., 2014; Frampton *et al*., 2015; Baltrus *et al*., 2019; Pinheiro *et al*., 2019; Rooney *et al*., 2020; Holtappels *et al*., 2020).

LPSs are complex glycolipids that make up the surface leaflet of the outer membrane of gram-negative bacteria, forming a physical protective barrier. LPSs have three distinct domains: Lipid A that tethers the molecule to the outer membrane, the O-polysaccharide (OPS) that interfaces with the external environment and the core domain that links Lipid A to the OPS. The OPS can comprise two distinct polysaccharides the O-specific antigen (OSA) and/or the common O-polysaccharide antigen (CPA) and is structurally the most variable component of the LPS. One of the distinctions between the two OPS polysaccharides is that the CPA is exported via an ABC transporter-dependent pathway, while OSA synthesis follows the Wzx/Wzy-dependent pathway (Raetz and Whitfield, 2002). In many bacterial species, the OPS is responsible for the immunological variation between isolates and, for human and animal pathogens, subspecies classification is based on serotypes (King *et al*., 2009; DebRoy *et al*., 2016). Similarly, the structures of OPS in plant-pathogenic bacteria such as *P. syringae* are highly variable at the pathovar level (Ovod *et al*., 1997a). For *P. syringae*, the OPS appears to be comprised of the CPA (Mesarich *et al*., 2017; Kutschera *et al*., 2019a) with a backbone consisting of a tri- or tetra-saccharide repeating unit, comprising either L- or D-Rhamnose (Rha), or a combination of the two, with various linkages. These are decorated with side chains consisting of different sugars such as *N*-acetylglucosamine (GlcNAc), fucose (Fuc), Rha, and *N*-acetylfucosamine (FucNAc) (Ovod *et al*., 1997a; Zdorovenko and Zdorovenko, 2010). The OPS can also be methylated or acetylated to varying degrees (Zdorovenko *et al*., 2001). At least nine serotypes of *P. syringae* have been identified, and each differs in the structure of the OPS backbone and side-chain modifications (Zdorovenko and Zdorovenko, 2010). Although considerable effort in the past was devoted to attempts at relating serotype to pathovar identification and taxonomy, correlations were not consistently observed (Ovod *et al*., 1997b). Little is known about the biosynthesis of LPS in *P. syringae* or the genetic basis for the observed structural and immunological variability within the genus.

Transposon mutagenesis of *Psa* BV3 using Tn5 identified a set of mutations with a rough (R) colony phenotype (Mesarich *et al*., 2017). This phenotype is often associated with mutations in LPS biosynthesis. Indeed, the majority of the Tn5 inserts in these R-LPS mutants mapped to a gene cluster in *Psa* orthologous to the CPA biosynthetic pathway from *P. aeruginosa* (Mesarich *et al*., 2017). Furthermore, LPS was not observed in these mutants, suggesting CPA is the sole OPS in *Psa* (Hockett *et al*., 2017). Other recent papers have shown a relationship between OSA and tailocin sensitivity among the Pseudomonads (Carim *et al*., 2020), directly identified components of CPA biosynthesis in *P. syringae* through gene knockouts (Kutschera *et al*., 2019a) and increased resistance to tailocins (Kandel *et al*., 2020).

Here, we investigated the genetics of LPS biosynthesis in *Psa*. We characterized the CPA locus and the orthologous region in the different *Psa* BVs, *P. syringae* and the closely related species *P. viridiflava*. We show an operon from this locus displays a high degree of variability consistent with horizontal gene transfer rather than a vertical evolutionary history which accounts for the high degree of structural variation of LPS observed in this species complex. Furthermore, the relationship between this component of the CPA locus and sensitivity to tailocins was highly correlated.

Results

Major LPS biosynthesis genes in Psa *BV3 are shared with* P. aeruginosa

In *P. aeruginosa* PAO1, the genes and operons responsible for the biosynthesis of Lipid A, the core LPS and the

OPS tend to be co-located and have been well annotated and characterized (King *et al*., 2009; Lam *et al*., 2011). We identified the key loci containing the majority of the LPS biosynthetic genes in *Psa* BV3 using BLASTx with *P. aeruginosa* PAO1 orthologues (Fig. 1A and Table 1). Amino acid similarity to *P. aeruginosa* PAO1 orthologues of the lipid A, core LPS, and Rha biosynthetic pathways in the CPA locus is relatively high (Table 1). In contrast, *Psa* genes putatively coding for other components of the CPA, such as the *wzm*/*wzt*/*wbpX* orthologues, are more divergent and have poor or no significant BLASTx hits. Evidence for an OSA biosynthetic cluster was not found, apart from genes in the *wbpK-M* locus, which is also involved in CPA biosynthesis (Table 1). The co-location of genes annotated as ABC transporters and glycosyltransferases (GT) with both the D- and L-Rha biosynthetic pathways suggests that the CPA is the predominant OPS in *Psa* BV3 (Fig. 1A).

Bioinformatic identification of the CPA locus in Psa BV3

Identifying the CPA locus in *P. syringae* has been challenging due to the lack of similarity to *wzm*/*wzt*/*wbpX* orthologues (Kutschera *et al*., 2019a). Previous work

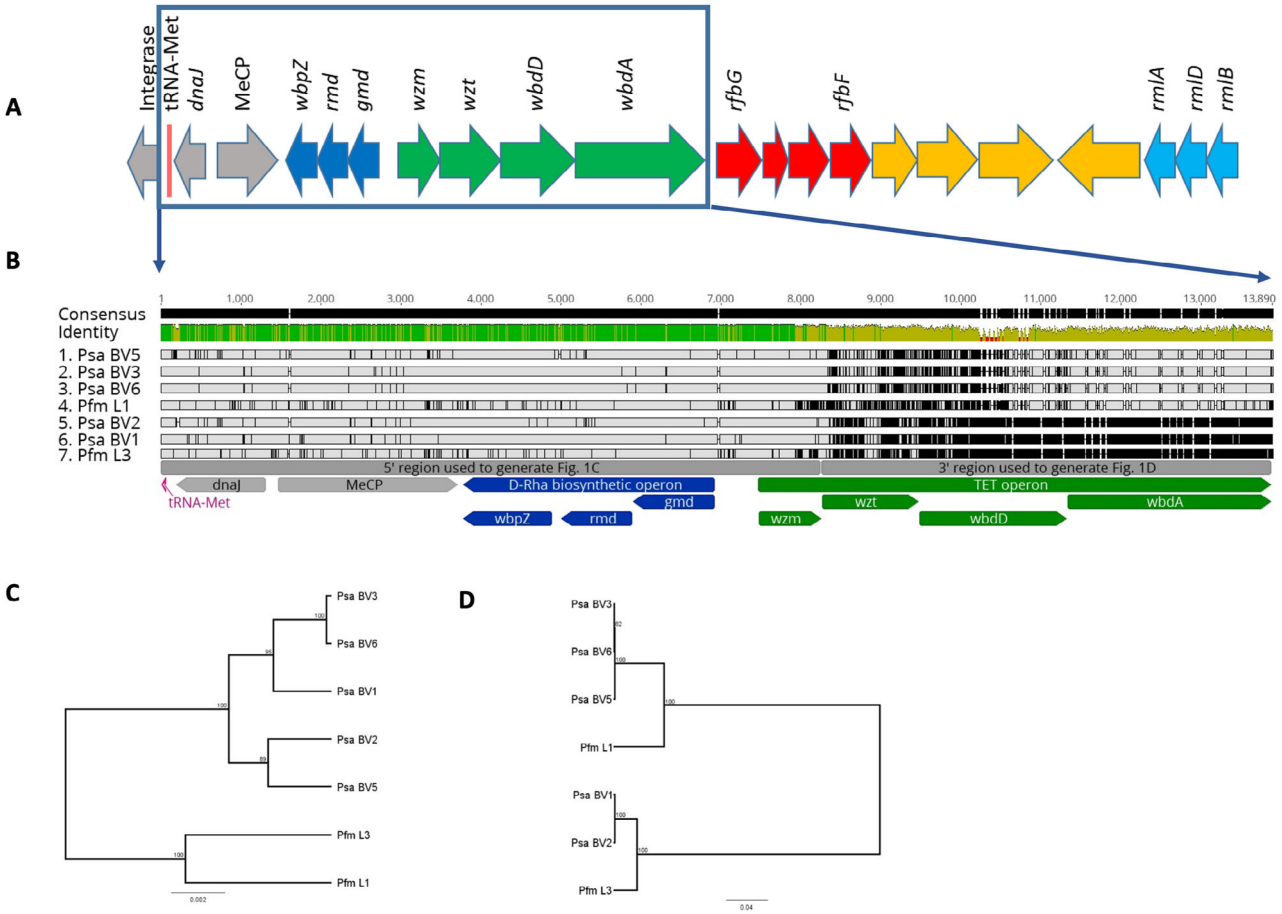

Fig. 1. The common polysaccharide antigen (CPA) locus from *Pseudomonas syringae* pv. *actinidiae* (*Psa*) and *P. syringae* pv. *actinidifoliorum* (*Pfm*).
A. The genetic structure of the CPA locus in *Psa* ICMP18884 (BV3). The four operons annotated are: the D-Rha biosynthesis operon (dark blue; IYO_23020-30), CPA transport, extension, and termination (TET) operon (green; IYO_23000-15), synthesis of unknown sugar operon (red; IYO_22980-95), L-Rha synthesis operon (light blue; IYO_22945-55), neighbouring syntenic genes that are not believed to be part of this functional cluster are shaded grey (IYO_023035-50) or yellow (IYO_022960-75) (see Table 2 for details).
B. Nucleotide alignment of the conserved D-Rha biosynthesis and polymorphic TET operons of *Psa* and *Pfm*. The CPA locus beginning at the syntenic conserved tRNA-Met through *wbdA* of the TET locus for representatives of the *Psa* biovars (BV1, ICMP 9617; BV2, ICMP 19071; BV3, ICMP 18884; BV5, MAFF 212063; and BV6, MAFF 212141) and *Pfm* lineages (L1, ICMP 18803; L3, ICMP 18807) aligned in Geneious v11. Grey regions indicate nucleotide identity and black lines and regions indicate nucleotide divergence. The consensus identity in green (high identity), yellow (low identify) and red (no alignment) is displayed above the aligned sequences. Flanking DnaJ and MeCP genes are annotated in grey, D-Rha biosynthesis operon and its genes are annotated in dark blue, and TET operon and its genes annotated in green.
C. UPGMA tree of the CPA locus from 5′ region up to and including *wzm* in (B).
D. UPGMA tree of the CPA locus from 3′ region from *wzt* to *wbdA* in (B).

Table 1. Loci involved in lipopolysaccharide (LPS) biosynthesis in *Pseudomonas syringae* pv. *actinidiae* BV3.

LPS component	*Psa* BV3 gene locus-tag	*P. aeruginosa* PAO1 orthologues	Amino acid identity	Gene name	*Psa* R-LPS phenotype[a]
Lipid A	IYO_000255	PA0011	80%	*lpxL*	N/A
Lipid A	IYO_007660-75	PA3643-6	55%–63%	*lpxA-D*	N/A
Lipid A	IYO_016185-225	PA3552-59	87%–94%	*arnA-F*, *arnT*	N/A
Core	IYO_025525-640	PA5001-12, PA4988,	66%–86%		Yes
CPA	IYO_005330	PA5448	37%	*wbpY*	Yes
CPA	IYO_008990-9000	PA3141, PA3145-6	40%–74%	*wbpK-M*	Yes
CPA	IYO_022945-023030	PA5447-59, PA5322	55%–80%[b]		Yes

a. R-LPS, Rough LPS.
b. D- and L-Rha biosynthetic genes only.

Table 2. Gene annotations of *Pseudomonas syringae* pv. *actinidiae* BV3 common LPS locus.

Gene annotation	Operon colour[a]	*P. aeruginosa*	*E. coli*	Function	Gene ID	Protein_ID	R-LPS[b]
dTDP-glucose 4,6-dehydratase	Light blue		*rmlB*	L-Rha biosynthesis	IYO_022945	AKT32330.1	
dTDP-4-dehydrorhamnose reductase	Light blue		*rmlD*	L-Rha biosynthesis	IYO_022950	AKT32331.1	
Glucose-1-phosphate thymidylyltransferase	Light blue		*rmlA*	L-Rha biosynthesis	IYO_022955	AKT32332.1	
Hypothetical protein	Orange			Unknown	IYO_022960	AKT32333.1	
Hypothetical protein	Orange			Unknown	IYO_022965	AKT32334.1	
Amine oxidase	Orange			Unknown	IYO_022970	AKT32335.1	
Membrane protein	Orange			Unknown	IYO_022975	AKT32336.1	
Glucose-1-phosphate cytidylyltransferase	Red		*rfbF*	Synthesis of unknown sugar	IYO_022980	AKT32337.1	
Glycosyl transferase	Red			Synthesis of unknown sugar	IYO_022985	AKT32338.1	
NAD-dependent epimerase/ dehydratase	Red		*galE*	Synthesis of unknown sugar	IYO_022990	AKT32339.1	
CDP-glucose 4,6-dehydratase	Red		*rfbG*	Synthesis of unknown sugar	IYO_022995	AKT32340.1	
Glycosyl transferase family 1	Green	*wbpX*	*wbdA*	Chain elongation	IYO_023000	AKT32341.1	
SAM-dependent methyltransferase	Green		*wbdD*	Chain termination	IYO_023005	AKT32342.1	Yes
Sugar ABC transporter ATP-binding protein	Green	*wzt*	*wzt*	Transport	IYO_023010	AKT32343.1	Yes
ABC transporter	Green	*wzm*	*wzm*	Transport	IYO_023015	AKT32344.1	Yes
GDP-D-mannose dehydratase	Blue	*gmd*	*gmd*	D-Rha biosynthesis	IYO_023020	AKT32345.1	Yes
GDP-6-deoxy-D-lyxo-4-hexulose reductase	Blue	*rmd*	*rmd*	D-Rha biosynthesis	IYO_023025	AKT32346.1	
Glycosyl transferase family 1	Blue	*wbpZ*		D-Rha biosynthesis	IYO_023030	AKT32347.1	Yes

a. Operon colour used in Fig. 1.
b. R-LPS, Rough LPS phenotype.

identified five R-LPS mutants by Tn5 mutagenesis that had inserts in a region with homology to the CPA biosynthetic pathway from *P. aeruginosa* PAO1 (Mesarich *et al*., 2017). Bioinformatic analysis of this region revealed a locus of 18 genes (Fig. 1A). These genes were arranged in operons predicted to be involved in the synthesis of L-Rha, D-Rha, an unknown sugar, an ABC transporter complex involved in the transport of the CPA, a bifunctional glycosyltransferase, an O-methyltransferase, and a region of unpredicted function (Table 2). Of the two genes annotated as ABC transporters, the first (IYO_023015) has homology to the ABC permease superfamily gene *wzm*, while the second (IYO_023010) has an N-terminal ATPase domain with a C-terminal *wzt*-like domain (hereafter called *wzt*). The latter domain binds to the non-reducing terminal modification of the sugar chain and is thus specific for the transported molecule (Cuthbertson *et al*., 2007). The GT gene (*wbdA*, IYO_023000) on the same operon as the two ABC transporters has two GT4 domains, implying it catalyses two distinct glycosyl transfer reactions. It is homologous to *wbdA* in *E. coli* (formerly known as *mtfB*), a functionally

characterized mannosyltransferase, which has been shown to direct the extension of the O9-specific polysaccharide chain by synthesizing, then polymerizing, the tetra-saccharide repeat (Liston *et al*., 2015). The adjacent gene (IYO_023005) on the *Psa* BV3 operon is annotated as an O-methyltransferase. In *E. coli*, the LPS oligosaccharide chain extension, catalysed by WbdA, is terminated by a dual methyltransferase/kinase enzyme (WbdD) (Mann *et al*., 2019). It appears therefore that this operon possesses genes required for the *t*ransport, *e*xtension, and *t*ermination of the backbone oligosaccharide chain of the CPA in *Psa* BV3 (hereafter referred to as the TET operon). This is the first time this operon has been identified in isolates of the *P. syringae* species complex.

Two different versions of the TET operon are present in Psa *and* Pfm

The CPA locus from representatives of all five *Psa* BVs and two lineages of *Pfm* were identified and compared. The TET operon, genes for D-Rha biosynthesis, and regions coding for a chemotactic receptor, a DnaJ molecular chaperone and a tRNA-Met were shared and could be aligned (Fig. 1B). The latter three genes were syntenic in all genomes but are not part of the CPA locus. The region including the D-Rha biosynthetic pathway and the first gene (*wzm*) in the TET operon (5′ region) is well conserved with few SNPs and a phylogenetic tree (Fig. 1C) closely matched the topology of a tree generated from seven conserved genes (Sawada *et al*., 2016). In contrast, the 3′ region, from the gene encoding the ABC transporter ATPase (*wzt*) of the TET operon is more variable, representing two groups of divergent sequences. One group includes *Psa* BVs 1 and 2, and *Pfm* L3, while the other includes *Psa* BVs 3, 5, and 6, and *Pfm* L1. A phylogenetic tree of this region (Fig. 1D) resolved into two clades that did not match the topology of Fig. 1C, or the phylogeny generated from the core genome (Supporting Information Fig. S1). These results suggest that variation at the TET operon is driving diversity at the CPA locus in *Psa* and *Pfm*.

LPS from Psa *and* Pfm *has different biochemical properties*

To assess whether genetic variation in the TET operon results in variation of the biochemical properties of LPS, we extracted LPS from *Psa* and *Pfm* using the method of Westphal and Jann (1965). Resolution of the extracted LPS by SDS-PAGE revealed the classic ladder pattern characteristic of bacterial LPS molecules, a reflection of the length and charge micro-heterogeneity of the O-linked saccharides (Jann *et al*., 1975). Comparison of the LPS between the five different BVs of *Psa* and two lineages of *Pfm* revealed two patterns based on differences in the molecular weight range and spacing between bands (Fig. 2A). LPS from *Psa* BV1, BV2 and *Pfm* L3 formed one group, which was characterized by a broad range of molecular weights, especially in the higher molecular mass range. In contrast, *Psa* BV3, BV5, BV6 and *Pfm* L1 formed a second group that had a lower range of molecular weights and narrower spacing between bands (Fig. 2A). The two electrophoretic pattern groups reflect the broad clusters evident in the TET operon tree (Fig. 1D), suggesting the TET operon plays a significant role in defining the electrophoretic properties of LPS. Banding patterns within a group were not identical, suggesting that they may differ in decoration of the back bone with side-chain sugars and/or acylation. Therefore, the genetic and biochemical data indicate that the CPA locus identified in *Psa* and *Pfm* contributes to LPS biosynthesis in these *P. syringae* pathovars.

Purified polyclonal antibodies against LPS from Psa *and* Pfm *do not cross react*

Western blots of the various LPS preparations from isolates of *Psa* and *Pfm* were probed with each affinity-purified polyclonal antibody preparation (Fig. 2B). All affinity-purified polyclonal antibodies showed a high degree of specificity, with little cross-reactivity against closely related isolates. The anti-*Psa* BV3 antibody preparation was the most specific, reacting with BV3, BV5, and only weakly to BV6 LPS (Fig. 2Bi). The weak binding to the *Psa* BV6 LPS and the slightly different *Psa* BV6 LPS profile (Fig. 2A) suggest a subtle difference in the CPA decoration. There was no cross-reactivity of the *Psa* BV3 antibody to the *Psa* BV1, BV2, or *Pfm* LPS preparations (Fig. 2B). The lack of binding of the anti-Psa BV3 antibody to *Pfm* L1 LPS (which has an electrophoretic profile more similar to BV3 LPS than *Pfm* L3) is likely due to the fact that antibodies that bind to epitopes shared by both BV3 and *Pfm*L1 were depleted by the affinity chromatography purification process used. The anti-BV1 antibody preparation reacted strongly with both *Psa* BV1 and BV2 LPS, as expected based on the close genetic identity between their TET loci (Fig. 2Bii). There was also weak cross-reactivity of *Psa* BV1 with *Psa* BV3 and BV5 LPS preparations (Fig. 2Bii). Interestingly, the *Pfm* L1 antibody had a slight cross-reactivity with *Pfm* L3 but not with the *Psa* isolates in the same grouping (Fig. 2Biii). This may be due to side-chain modifications that are common between the two CPA polysaccharides. These results further support the different grouping of LPS between these strains but also indicate that antibody specificity is influenced by both backbone structure and side-chain decorations.

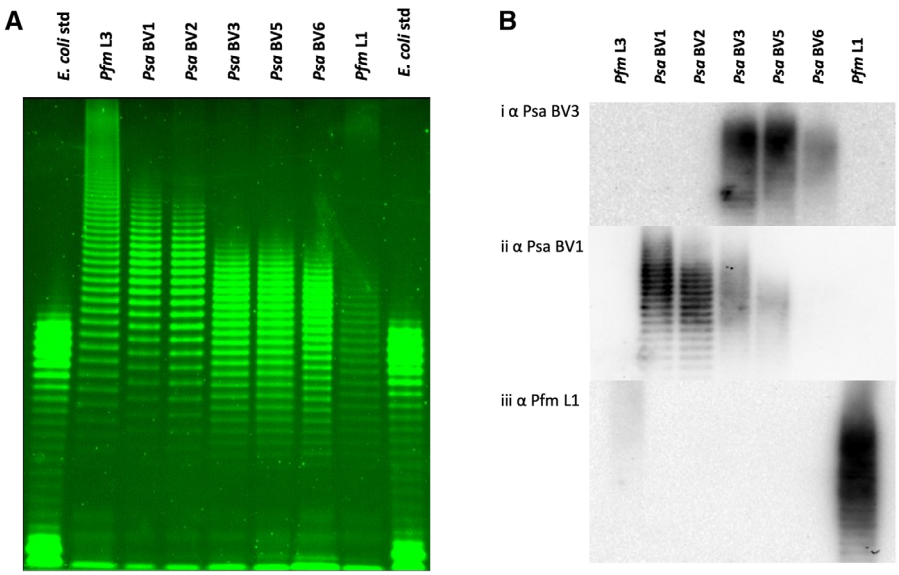

Fig. 2. LPS profiles of *Pseudomonas syringae* pv. *actinidiae* (*Psa*) and *P. syringae* pv. *actinidifoliorum* (*Pfm*).
A. Pro-Q™ Emerald 300 staining of lipopolysaccharide (LPS) preparations on a NuPAGE 4%–12% gradient bis-tricine SDS gel from representatives of *Pfm* lineages (L3 ICMP 18807, lane 2; L1 ICMP 18803, lane 8), *Psa* biovars (BV1 ICMP 9617, lane 3; BV2 ICMP 19071, lane 4; BV3 ICMP 18884, lane 5; BV5 MAFF212063, lane 6; BV6 MAFF 212141, lane 7), with *Escherichia coli* standards (Std; lanes 1 and 9). A total of 0.5–15 μl LPS extract for each sample (normalized by trial runs) was applied per lane.
B. Western blot of LPS extracts from representatives of *Psa* biovars and *Pfm* lineages run on a NuPAGE 4%–12% gradient bis-tricine SDS gel, obtained by probing with polyclonal antibodies to *Psa* BV3 ICMP 18884 (Bi), *Psa* BV1 ICMP 9617 (Bii), or *Pfm* L1 ICMP 18803 (Biii) in a 5000:1 ratio.

The TET operon determines the variability of LPS banding in Psa

To confirm whether the TET operon, expressing the ABC transporter (*wzt*), putative oligosaccharide chain elongation GT (*wbdA*), and the o-methyltransferase (*wbdD*), are responsible for the different LPS profiles, this operon was deleted in *Psa* BV1 (Fig. 3A; dark green region, Supporting Information Fig. S2) and replaced with that from *Psa* BV3 (Fig. 3A, blue region, Supporting Information Fig. S2). The *Psa* BV1 TET operon knock-out (Δ*LPS* KO) lacked LPS and possessed a rapid sedimentation phenotype, but had a very weak R-LPS colony morphology, as observed for the BV3 mutants (Fig. 3B; Supporting Information Figs. S3A and S4). *Psa* BV1 with the BV3 LPS knocked back in (four knock-in lines, Δ*LPS* + *LPS*_BV3 #1–2, #1–4, #2–1, and #2–5), but not for the KO revertants that failed to retain this region (e.g. #1–3), restored these LPS-associated phenotypes (Fig. 3B, Supporting Information Figs. S3A, B and S4). Furthermore, the LPS profile was identical to that of wild-type BV3, proving this locus codes for the genes involved in generating the BV-specific LPS oligosaccharide ladder. A Western blot of the LPS gel of these strains was probed with the *Psa* BV3 antibody (Fig. 3C), which showed that transfer of the TET locus from *Psa* BV3 to the *Psa* BV1 Δ*LPS* KO also transferred the antibody specificity. In summary, this genetic TET-swap analysis provided direct evidence that these genes were necessary and sufficient for the differences in LPS between these strains.

LPS is required for full pathogenicity of Psa *in kiwifruit plantlets*

Previously, LPS mutations have been found to affect host colonization by *P. syringae* (Kutschera *et al*., 2019a). To investigate the role of LPS in the virulence or pathogenicity of *Psa*, we infected kiwifruit plantlets with *Psa* BV3 R-LPS Tn5 mutants (Δ*wbpL*, Δ*wzm*, Δ*wbdD*, Δ*wzt*, and Δ*gmd*) (Mesarich *et al*., 2017) and the *Psa* BV1 knock-out (Δ*LPS*), two knock-in (Δ*LPS* + *LPS_BV3* #1–4 and #2–1) and two knock-out revertant (Δ*LPS-LPSrev* #1–3 and #2–4) mutants, along with their wild-type counterparts. All LPS mutants showed at least a log reduction in growth *in planta* compared to wild-type strains, indicating that LPS is required for full host colonization (Fig. 4A and B) and symptom development (Supporting Information Fig. S5A and B). Meanwhile, the knock-in BV1Δ*LPS* + *LPS_BV3* strains with complemented LPS production restored wild-type growth to the Δ*LPS* mutant (Fig. 4B; Supporting Information Fig. S5B) and this did not occur in the strains that had reverted to Δ*LPS*.

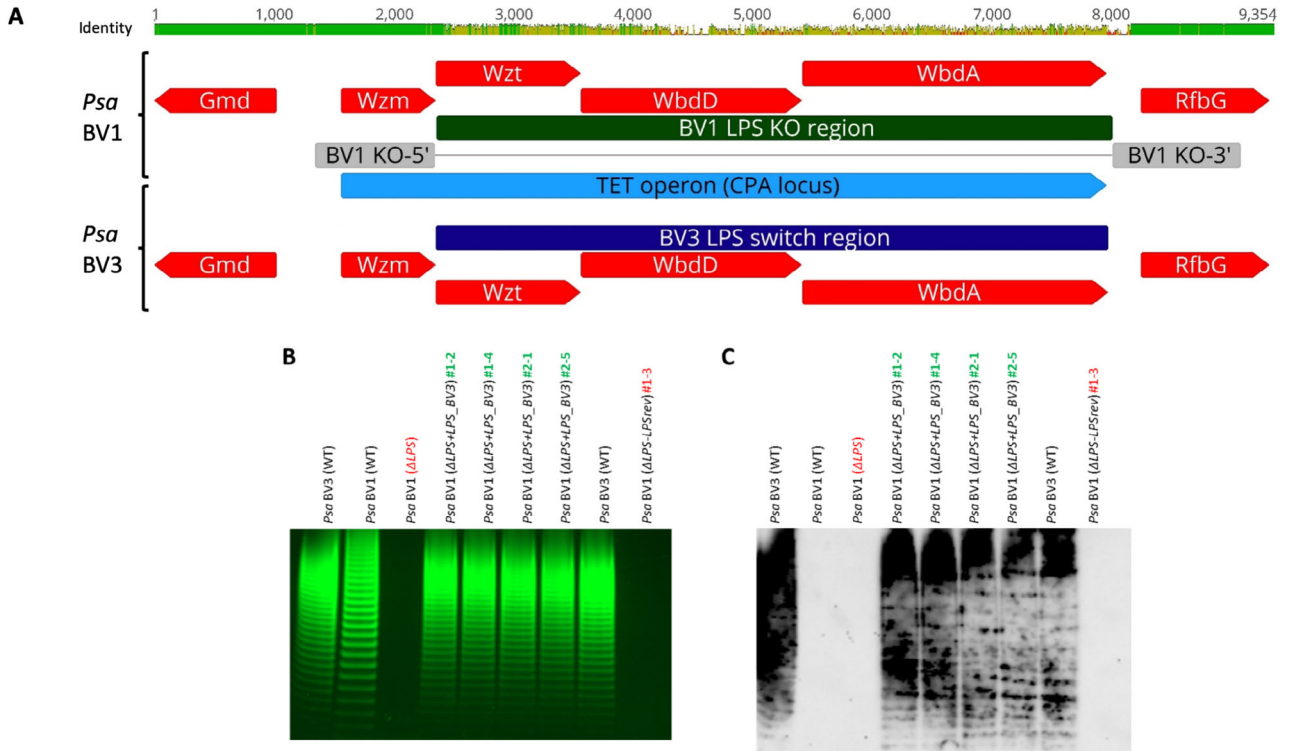

Fig. 3. Effects of CPA TET operon swap on LPS banding and immunological recognition in *Pseudomonas syringae* pv. *actinidiae* (*Psa*).
A. Genetic polymorphism of the TET operon for *Psa* BV1 (ICMP 9617) versus BV3 (ICMP 18884). DNA sequences were aligned in Geneious v11. Nucleotide identity is shown on the top bar, the TET operon is annotated in light blue, coding sequences in red with predicted biochemical function indicated, the original TET operon from BV1 indicated in dark green with upstream (KO-5′) and downstream (KO-3′) regions for generating the LPS TET operon knock-out in grey, and the TET operon swap region by knock-in from BV3 indicated in dark blue.
B. LPS profiles of *Psa* BV3 (lane 1 and lane 8), BV1 (lane 2), BV1 TET operon knockout (Δ*LPS*; lane 3), four BV1-to-BV3 TET operon knock-in complemented isolates (Δ*LPS* + *LPS*_BV3 #1–2, #1–4, #2–1, and #2–5; lanes 4–7), and one BV1 revertant to knock-out isolates (ΔLPS-LPSrev #1–3; lane 9). Pro-Q™ Emerald 300 staining of LPS preparations on a 4%–12% gradient Tris-glycine SDS gel. LPS extract (15 μl) for each sample was applied per lane.
C. Immuno-blot of LPS extracts from wild-type, knock-out (KO), KO-complemented, and KO-revertant strains run on a gradient SDS-PAGE gel as for (B), probed with polyclonal antibodies to *Psa* BV3 in a 5000:1 ratio.

The TET operon from P. syringae *isolates is highly variable but correlates with LPS*

Having identified the TET operon in *P. syringae*, we set out to investigate this operon in a range of isolates the *P. syringae* species complex and closely related plant-associated *Pseudomonas* species. In *P. syringae*, the composition of the CPA backbone (D- and/or L-Rha), the number of sugars in the repeat, and the bonds linking the sugars within the oligosaccharide, vary between different *P. syringae* isolates (Ovod *et al*., 1997a; Zdorovenko and Zdorovenko, 2010). BLASTx and conserved domain database (CDD) searches identified the CPA locus in other *P. syringae* pathovars and epiphytic isolates. We also included several *P. viridiflava* isolates (See Supporting Information Table S1 for details of all isolates analysed). Comparison of these loci revealed variation in the sugar biosynthetic pathways comprising the CPA locus, including the TET operon (Supporting Information Fig. S6). In some *P. syringae* isolates, the GT and O-methyltransferase genes were fused (Supporting Information Fig. S6). The TET operon showed a high degree of sequence variation between *P. syringae* pathovars and isolates. Variation in CPA sugar biosynthetic pathways and the sequence divergence of the TET operon made the identification of this region in *P. syringae* challenging, but as noted previously, the CPA locus was consistently located adjacent to genes encoding a chemotactic receptor, DnaJ molecular chaperone and a tRNA-Met (Fig. 1A). A gene encoding an integrase was often located adjacent to the tRNA-Met in an orientation reminiscent of an integron (Domingues *et al*., 2012; Gillings, 2014). Given that tRNAs are often sites for integration of mobile elements, this might explain the modular and variable nature of the CPA locus in *P. syringae*. However, a canonical integron structure was not found using programs such as integron finder (Cury *et al*., 2016).

Phylogenetic analysis of the concatenated proteins from the TET operon generated a tree with five main clades (including the two clades identified in *Psa* and *Pfm*), each representing different sets of alleles of this operon

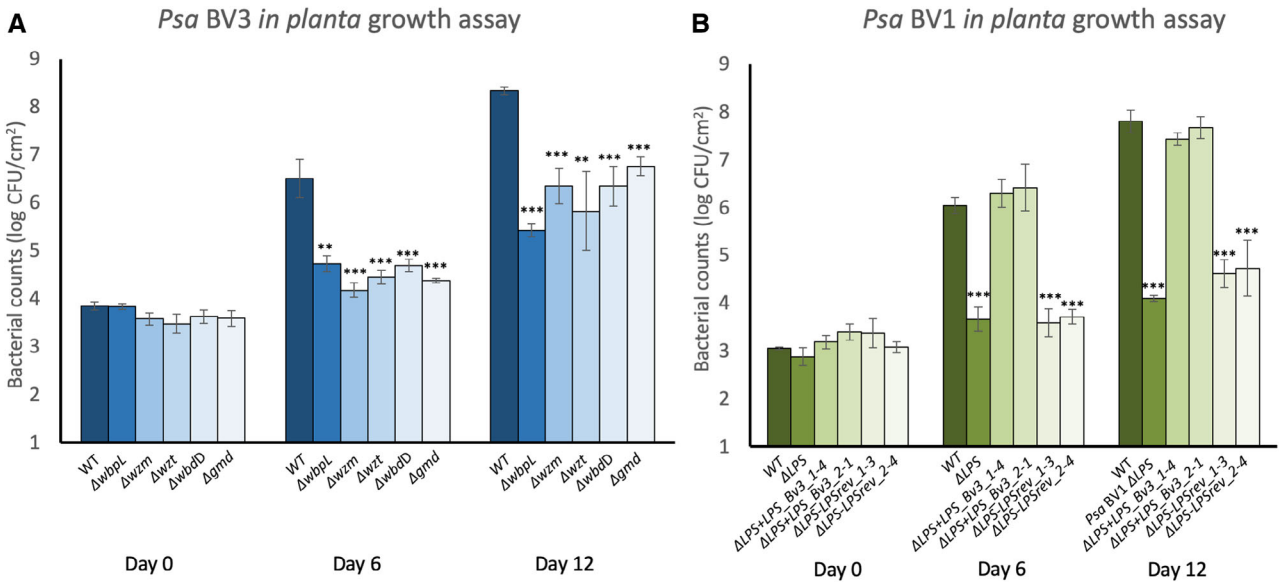

Fig. 4. The CPA TET operon is required for full pathogenicity of *Pseudomonas syringae* pv. *actinidiae* (*Psa*) in host plants.
A. *P*sa BV3 or BV3 R-LPS mutants (Mesarich *et al*., 2017) were flood-inoculated at ~5 × 10^6 CFU/ml on *Actinidia chinensis* var. *chinensis* 'Zesy002', and bacterial growth was determined at 0, 6, and 12 days post-inoculation. Error bars represent standard error of the mean from four pseudo-biological replicates. Asterisks indicate results of Student's *t*-test between selected sample and wild type; ***P* < 0.01, ****P* < 0.001). The experiment was conducted three times with similar results.
B. *P*sa BV1, BV1 LPS knock-out mutant (Δ*LPS*), two independent BV1 knock-outs complemented by knock-in with LPS from BV3 (+LPS_BV3 #1-4 and #2-1), and two independent BV1 revertant-to-knock-out LPS (-LPSrev #1-3 and #2-4) were flood-inoculated at ~5 × 10^6 CFU/ml on *A. chinensis* var. *chinensis* 'Hort16A', and bacterial growth was determined at 0, 6, and 12 days post-inoculation. Error bars represent standard error of the mean from four replicates. Asterisks indicate results of Student's *t*-test between selected sample and wild type (*Psa* BV3); ****P* < 0.001. The experiment was conducted twice with similar results.

from the *P. syringae* and *P. viridiflava* species complexes (Fig. 5A). As observed with *Psa* and *Pfm* isolates, the topology of the tree made from these sequences is very different from the corresponding tree generated from five core genes (*gyrB*, *rpoA*, *gapA*, *pgi*, *acnD*) from the respective genomes (Supporting Information Fig. S1). This indicates that the TET operon has an evolutionary history driven by recombination or horizontal gene transfer that is distinct from the evolution of the core genome.

Since genetic variation in the CPA between even closely related isolates of *Psa* and *Pfm* is reflected in different LPS profiles, we performed a broader analysis of LPS profiles across different clades of *P. syringae* (Fig. 5A). Eleven isolates of *P. syringae* were chosen, representing four TET operon phylogenetic clades. The banding patterns were different for all isolates, but similarity within clades was observed. Notably, the spacing between bands was clearly similar within clades but varied between them (Fig. 5B). Interestingly, the range of molecular weights of different LPS molecules within clades was highly variable, suggesting the efficiency of the chain terminating enzyme (WbdD) varies within a clade. While considerable variability has been demonstrated in *P. syringae* CPA, the functional relevance of this is less well understood.

Correlation between tailocin sensitivity and TET operon variability

Like phages, many R-type syringacins (tailocins) use LPS as a receptor. Recently the R-syringacin killing and sensitivity spectra for a diverse range of *P. syringae* isolates were characterized (Baltrus *et al*., 2019). A feature of both spectra is that dendrograms generated from the killing and sensitivity matrices do not match MLST phylogenetic trees (Baltrus *et al*., 2019). Since LPS is a likely receptor for R-syringacins, we hypothesized that there might be a correlation between the patterns of variation in tailocin sensitivity within *P. syringae* isolates and the genetic variation in the TET operon responsible for the structure of the CPA backbone.

To test this hypothesis, we generated a UPGMA phylogenetic tree from the TET operons from 29 of the isolates tested for tailocin killing and sensitivity by Baltrus *et al*. (2019). This was compared to a hierarchical clustering tree generated from the sensitivity profile of the same isolates using a tanglegram (Fig. 6A). Tanglegrams compare phylogenetic trees to determine how similar they are and correlation coefficients can be calculated from the similarity between different pairs of trees (Galili, 2015). The correlation

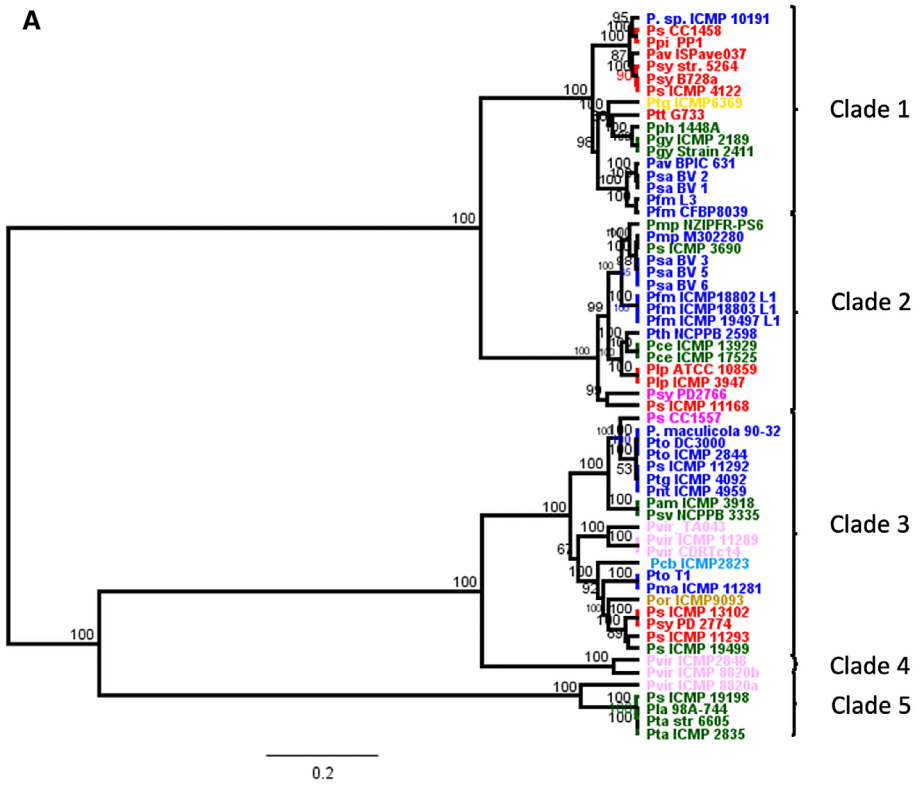

Fig. 5. A. Phylogenetic comparison of TET operons from various *Pseudomonas syringae* strains. Amino acid sequences from three proteins of the CPA locus (Wzt, WbdD and WbdA) were aligned in Geneious v11 and neighbour-joining phylogenetic trees built for their TET operons. Strains were grouped into numbered clades as indicated. Strains are coloured according to their core genome phylogenies as previously described (Dillon *et al*., 2019b): phylogroup 1 blue; phylogroup 2 red; phylogroup 3 green; phylogroup 4 orange; phylogroup 5 light-blue; phylogroup 6 yellow; phylogroup 7 pink; phylogroup 10 mauve.
B. LPS profiles of *Pseudomonas syringae* representing phylogenetic clades for the TET operon. Pro-Q™ Emerald 300 staining of lipopolysaccharide (LPS) preparations on a 4%–12% gradient Tris-glycine SDS gel from representatives of *P. syringae* strains from Supporting Information Table S1 (top to bottom, lanes 1–11), with *Escherichia coli* control (Std, lane 12). Banding patterns were grouped into clades on their designations from (A). A total of 2–15 μl LPS extract for each sample (normalized by trial runs) was applied per lane.

coefficient between the sensitivity and TET operon trees was 0.987, indicating a high degree of congruence (Supporting Information Fig. S7). Both trees comprise two main clades, and there was a 100% correlation among the isolates between the clades in both trees. In contrast, tanglegrams between either the sensitivity profile or the TET operon and an MLST phylogenetic tree had low correlation coefficients of 0.011 and −0.003, respectively, indicating poor congruence (Fig. 6B and C; Supporting Information Fig. S7). These results suggest a strong relationship between tailocin sensitivity and the structure of the CPA oligosaccharide of LPS in *P. syringae*. They provide further evidence that LPS is a tailocin receptor in *P. syringae*, explaining the complex host range observed for these proteins (Baltrus *et al*., 2019) and providing a plausible explanation for the diversification pattern of these loci.

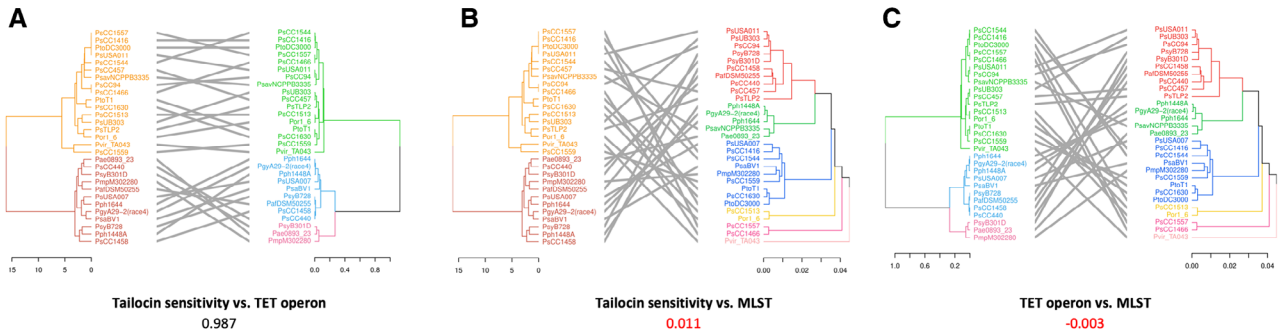

Fig. 6. Tanglegram comparison of tailocin sensitivity, TET operon, and core gene MLST phylogenies.
A. Tanglegram of sensitivity matrix phylogeny (left) and TET operon phylogeny (right).
B. Tanglegram of sensitivity matrix phylogeny (left) and core gene MLST phylogeny (right).
C. Tanglegram of TET operon phylogeny (left) and core gene MLST phylogeny (right). Hierarchical clustering analysis using the ward.D2 method was used to build a tailocin sensitivity phylogeny from the sensitivity matrix provided in the study by Baltrus *et al*. (2019), which is transposed from a syringacin killing matrix. The TET operon phylogeny was produced by using the TET operon genome sequences of selected strains, assembled into a phylogeny using the UPGMA clustering method, as was the MLST phylogeny. The co-phenetic entanglement coefficients for each comparison are indicated below each panel title. Axes in each panel represent Euclidean distance. Colours represent broad clade groupings, with the cut-offs being Euclidean distances of 10, 0.5, and 0.02 for the sensitivity, TET, and MLST phylogenies respectively. This Euclidean cut-off for the MLST branches allows representative separation by phylogroup for the strains used.

Discussion

LPS is a highly complex macromolecule located on the surface of the bacterial cell wall that interfaces with the environment and other organisms. It is often used as a receptor or ligand for recognition by other bacteria, phages, bacteriocins and the defence system of host organisms. LPS is made up of a modular structure that can generate structural variability, particularly in the OPS, which can help bacteria resist parasitic organisms, toxins and host defences (King *et al*., 2009). The structure and function of LPS from human and animal bacterial pathogens have been explored in depth where it has been shown that LPS interacts directly with the host immune system and hence immunity is a strong driver for genetic variation at loci coding for LPS (Lerouge and Vanderleyden, 2002; Maldonado *et al*., 2016).

In contrast, the role of LPS in plant-pathogenic and epiphytic bacteria is less clear. In this study, we have identified the CPA locus in *Psa* and shown it is responsible for the biosynthesis of the predominant OPS in *P. syringae*. The locus is highly modular with operons predicted to be involved in the biosynthesis of various sugars, although only those for L-Rha and D-Rha have been convincingly identified through similarity at the protein level. The TET operon that codes for proteins involved in the polymerization and transport of the backbone oligosaccharide through the inner membrane was also identified for the first time in *P. syringae*. The TET operon was present in the majority of *P. syringae* and *P. viridiflava* CPA loci examined. Phylogenetic analysis of three of the proteins in the TET operon revealed five distinct clades, which most likely reflect the different repeating unit structures of the CPA Rha-backbone oligosaccharide. There are two elements that contribute overall to the structural variability of the CPA in *P. syringae*. One is the nature of the backbone oligosaccharide, which can be tri- or tetrasaccharides of either D-Rha, L-Rha or both, linked by α1-2, α1-3, or β1-4 bonds (Ovod *et al*., 1997a). The other is the side-chain decoration, which is usually a single sugar residue attached by a variety of different linkages. In addition, acetylation is a common back-bone modification. Unfortunately, it is not possible to directly correlate the considerable structural data known about *P. syringae* LPS accurately with the clades resolved in Fig. 5A because the isolates for which structural LPS information is known are not those that have been sequenced (Zdorovenko and Zdorovenko, 2010).

The mechanism by which the different operons within the CPA locus are shuffled between *P. syringae* isolates to generate the observed structural variability could occur via homologous recombination or insertion via an integron-like cassette. The structure of the CPA locus in *Psa* BV3 resembles that of an integron, although an intact phage-like integrase adjacent to the tRNA-Met was not present in all other *P. syringae* isolates. In addition, a classic integron promoter and *attC* insertion sequences were not found using programs such as integron finder. The presence of operons from *P. viridiflava* in the phylogenetic trees suggest that the mechanism of recombination between isolates is not exclusive to the *P. syringae* species complex, but also includes other closely related species such as *P. viridiflava* that share the same ecological (plant-associated) niche. There did not appear to be any obvious geographical bias for any of the CPA clades. While this study is unlikely to be an exhaustive identification of TET operon variants, a significant proportion of available *P. syringae* whole genome sequences

collected from isolates from a wide range of geographical locations were analysed. Since members of four clades were isolated recently from kiwifruit in New Zealand, the TET operon alleles identified are likely to be ubiquitous among *P. syringae* populations.

The variation at the TET locus is also reminiscent of that at the capsule locus within the *Klebsiella pneumoniae* clonal group 258 (Wyres *et al*., 2015). In this case, it has been shown that extensive intra-clonal variation at the capsule polysaccharide synthesis locus is mediated by large-scale recombination events. This has been responsible for generation of the 78 immunologically distinct capsule variants which have been described in *K. pneumoniae* (Wyres *et al*., 2015). A similar mechanism may explain the variation observed for the TET operon and CPA locus in *P. syringae*.

Tailocins are a subset of bacteriocins derived from phage tail proteins that have been co-opted by host bacteria as a means for killing closely related bacterial isolates occupying the same ecological niche (Ghequire and De Mot, 2015). What has been demonstrated recently within *P. syringae* is the depth and complexity of both the killing and sensitivity spectra generated from a wide range of isolates (Baltrus *et al*., 2019). While it is clear that LPS is a receptor for some tailocins (Kutschera *et al*., 2019a; Kandal *et al*., 2020), a link between the sensitivity to tailocins and the structural variation in LPS has not been demonstrated until recently. Carim *et al*. (2020) have shown within the genus *Pseudomonas* that OSA composition and display are the most important contributors to tailocin sensitivity. Our results also indicate a strong but not perfect relationship between tailocin sensitivity and CPA within *P. syringae*. This suggests that killing by tailocins (and by inference infection by phages) may drive diversity in LPS structure in the wider *P. syringae* population. It appears less likely that recognition by plant defences is selecting for variation at the CPA locus. Instead, it has been shown that a medium chain 3-hydroxyl fatty acids of the lipid A molecule of LPS is detected by the plant pathogen associated molecular pattern receptor LORE (Kutschera *et al*., 2019b). It is interesting to note that the genetic variation driving differences at both the CPA locus and the tailocin killing spectrum in *P. syringae* appears to be mediated by localized recombination events (Baltrus *et al*., 2019).

As has been reported previously for other *P. syringae* LPS mutants (Kutschera *et al*., 2019a; Kandel *et al*., 2020), those in both the *Psa* BV3 and BV1 backgrounds displayed significantly reduced *in planta* growth compared to their wild-type strains at both 6- and 12-days post-inoculation (Fig. 4). The aggregation of LPS knockout isolates in solution may also affect the motility of these mutants *in planta* and could be responsible for reduced pathogenicity. Alternatively, LPS mutants may be more sensitive to host antimicrobial compounds. Although mutants lacking LPS have been shown to be highly resistant to particular bacteriophages and/or tailocins, the loss of pathogenicity probably ensures that strains completely lacking LPS are strongly selected against *in planta* (Kandel *et al*., 2020).

These findings, firstly that LPS is a trait conferred by a predictable locus, and secondly that LPS is required for pathogenicity, offer intriguing possibilities for a durable disease resistance program using bacteriophage/tailocin-mediated control. While the locus is open to recombination, the identification of the population of TET operon alleles present on a plant species may facilitate the development of a comprehensive mixture of bacteriophage/tailocin that covers the most common alleles to be deployed to increase efficacy and durability of this treatment by circumventing escape through recombination at the TET operon locus.

Experimental procedures

Bacterial isolates used in this study

Metadata for the bacterial isolates and genomes used in this study are listed in Supporting Information Table S1. Lysogeny broth (LB), and M9 minimal media (M9) (Sambrook and Russell, 2001) were supplemented with agar 1.5% (w/v) and 50 μg/ml kanamycin (Km) where required. *Escherichia coli* and *Pseudomonas* isolates were routinely cultured at 37°C and 28°C respectively. All kits and reagents were used, except where specified, in accordance with the manufacturer's instructions.

Bioinformatics

Bioinformatics analysis was carried out using the Geneious v11 platform (www.geneious.com). For unannotated genomes, the RAST pipeline was used for gene calling (Aziz *et al*., 2008). GenBank searches were carried out using BLAST (Boratyn *et al*., 2013). Sequences were searched for *attI* and *attC* motifs using Integron Finder https://github.com/gem-pasteur/Integron_Finder (Cury *et al*., 2016).

LPS purification

For small-scale preparations of LPS, the hot-phenol method was used (Westphal and Jann, 1965). Overnight bacterial cultures were resuspended in 500 μl phosphate-buffered saline (ThermoFisher Scientific, MA, USA) to an A_{600} of between 2 and 5. An equal volume of Tris-saturated phenol (Sigma-Aldrich, Mo, USA, P4557) was added and the sample was incubated at 68°C for 90 min

with intermittent vortexing. The supernatant was sequentially treated with DNase I (37°C) and RNase (65°C), each for 1 h. The samples were treated with phenol/chloroform/isoamyl alcohol, followed by chloroform/isoamyl alcohol and stored at −20°C. To generate antigen used for immunization and polyclonal antibody generation, large-scale extraction of LPS from *Psa* BV1 and BV3, and *Pfm* L1 was performed using the hot-phenol method of Maier and Brill (1978). Cells were harvested in late exponential phase, collected by centrifugation and freeze-dried for storage at −20°C.

LPS were resolved using 4%–12% premade NuPAGE™ Bis-Tris SDS gels on a Novex system with MOPS as the running buffer. Gels were stained using the Pro-Q™ Emerald 300 Lipopolysaccharide Gel Stain Kit (Molecular Probes, OR, USA). For Western blotting, gels were transferred to a polyvinylidene difluoride (PDVF) membrane (Millipore, Burlington, MA, USA). The anti-Psa antibodies (see below) were used at 1:5000 dilution and the Anti-Rabbit IgG-Peroxidase antibody (Sigma-Aldrich, St Louis, MO, USA) was used at 1:10 000 dilution. Chemiluminescence was developed using the Clarity Max Western ECL (Bio-Rad, Hercules, CA, USA).

Production of antibodies to Psa *biovars*

Heat-killed cells from *Psa* BV1 (ICMP 9617), *Psa* BV3 (ICMP 18884), and *Pfm* L1 (ICMP 18803) in Freund's complete adjuvant were each used to individually immunize two rabbits by subcutaneous injection of 10^8 cells. Rabbits were rested for 4 weeks and immunized every 2 weeks by three further injections. Blood was collected 1 week after the last injection, and rabbit IgG was purified from serum using ammonium sulphate fractionation and protein-A sepharose chromatography (Ey *et al*., 1978). These polyclonal antibodies were further purified by affinity chromatography through matrices attached to LPS extracted from the above isolates not used for immunization in each of the three cases. The aim of this step was to remove antibodies that bound to antigens in common with other isolates, to give an isolate-specific polyclonal antibody preparation. For example to purify antibodies specific for *Psa* BV3, IgG were passed through affinity columns with LPS from *Psa* BV1 and *Pfm* L1. For preparation of the matrices LPS was dissolved in buffer and oxidized using periodate. Excess periodate was removed by gel filtration using a PD10 column. Oxidized LPS was reacted with biotin hydrazide to biotinylate the LPS as per method sheet 28 020 (Thermo Fisher). LPS matrices for affinity chromatography were prepared by attachment of biotin-LPS to streptavidin-labelled sepharose columns. Biovar-specific LPS antibodies were purified by standard affinity chromatography as described by the manufacturer (GE Life Sciences, PA, USA).

LPS locus knock-out and knock-in

To generate the LPS TET operon (*wzt* – *wbdA*; ∼5.3 kb) deletion in *Psa* BV1 (ICMP 9617), a modified pK18mobsacB vector-based method was utilized (Kvitko and Collmer, 2011). DNA fragments containing the upstream (∼1 kb) and downstream (∼1 kb) regions of the LPS knock-out region were amplified using PCR with primer pairs PsaJ_LPS-KO_UP-F/PsaJ_LPS-KO_UP-R and PsaJ_LPS-KO_DN-F/PsaJ_LPS-KO_DN-R, respectively, with the UP-R and DN-F primers carrying added *Xba*I restriction enzyme sites (Supporting Information Table S2). Each PCR fragment was gel-purified using an EZNA gel extraction kit (Custom Science, Auckland, NZ, USA) and digested with *Xba*I, re-purified with an EZNA PCR product purification kit and ligated (to the *Xba*I-cut overhangs) to form a 2 kb KO fragment. The 2 kb fragment containing both the upstream and downstream fragments for the KO region was then re-amplified by PCR using primers PsaJ_LPS-KO_UP-F and PsaJ_LPS-KO_DN-R. This PCR product was cloned into the *Eco53*kI blunt-end restriction enzyme site of pK18mobsacB that had first been mutagenized to remove the non-MCS Eco53kI site to generate pK18BΔE (Schafer *et al*., 1994). The pK18BΔE vector carrying the ∼2 kb KO fragment, called pΔ*LPS*, was transformed into *E. coli* DH5α, plated on X-gal/IPTG/kanamycin LB agar for blue/white selection. Positive transformants were confirmed by Sanger sequencing (Macrogen, Seoul, South Korea). *Psa* BV1 was electroporated with the pΔ*LPS* construct and transformants were selected on LB agar with nitrofurantoin, cephalexin and kanamycin. Selected colonies were subsequently streaked onto LB agar containing 10% (w/v) sucrose to counter-select plasmid integration, forcing removal of the *sacB* gene, resulting in either revertants to wild-type or knock-outs. KOs were confirmed using colony PCR with primers PsaJ_LPS-KO_Check-F and PsaJ_LPS-KO_Check-R, with PCR products sent for Sanger sequencing with the nested cloning PsaJ_ LPS -KO_UP-F and PsaJ_ LPS -KO_DN-R primers, as well as using internal gene-specific primers. Selected colonies were also plated on kanamycin-containing medium to confirm loss of the plasmid backbone containing kanamycin resistance and the *sacB* gene.

To clone the knock-in (KI) construct of the *Psa* BV3 LPS TET operon for complementation of the *Psa* BV1 LPS TET operon knockout (*Psa* BV1 Δ*LPS*), the golden gate cloning system was used (Engler *et al*., 2009). Firstly, the destination vector was generated by restriction digestion using *Ase*I and *Nhe*I of pK18mobsacB to remove the multiple cloning site (MCS). This was replaced with a golden gate-compatible (*Bsa*I restriction enzyme site-flanked) MCS from pICH86988 using In-Fusion cloning according to kit instructions (Takara Bio,

USA) to generate a golden gate cloning-compatible version of the pK18mobsacB vector; pK18B-GG. The pK18B-GG vector was transformed into *E. coli* DH5α, plated on kanamycin LB agar and screened by *Bsa*I restriction digest. Positive transformants were confirmed by Sanger sequencing (Macrogen, South Korea). Entry-level vectors for the LPS-KI construct were generated for the LPS region from *Psa* BV3 (ICMP 18884), divided into four modules (modules 1–4), with overlap-fusions of the upstream (5′) and downstream (3′) regions of the *Psa* BV1 Δ*LPS* (for modules 1 and 4, respectively, with modules made by overlap PCR) and an additional module 5 for the downstream region of the *Psa* BV1 Δ*LPS* by PCR-amplification. These were cloned into pICH41021 with the cloning primers (Supporting Information Table S2) designed to synonymously mutate internal *Bsa*I, *Eco53k*I, and *Pst*I restriction enzyme sites (Supporting Information Fig. S2). These five LPS-KI modules in pICH41021 were then single-pot cloned (by golden gate assembly) into destination pK18B-GG to generate the LPS-KI vector: pLPSbv3. The pLPSbv3 vector was transformed into *E. coli* DH5α, plated on kanamycin LB agar and screened by nested colony PCR for correct assembly. Positive transformants were confirmed by Sanger sequencing (Macrogen). *Psa* BV1 Δ*LPS* was transformed with pLPSbv3 and transformants were selected on LB agar with nitrofurantoin, cephalexin and kanamycin. Selected colonies were subsequently streaked onto LB agar containing 10% (w/v) sucrose to counter-select plasmid integration, resulting in revertants to knock-out or LPS-complemented mutants. Complementation knock-in mutants were screened using colony PCR with primers for PsaJ_LPS-KO_Check-F and PsaJ_LPS-KO_Check-R, as well as gene-specific primers and sent for Sanger sequencing. Complemented knock-in mutants (Δ*LPS* + *LPS_BV3*) and non-complemented knock-out revertants (Δ*LPS-LPSrev*) were further confirmed by plating on kanamycin-containing agar to confirm loss of the *sacB* gene.

In planta *growth and symptomology of* Psa

Psa infection assays were based on those published previously with some modifications (McAtee *et al*., 2018). *A. chinensis* Planch. var. *chinensis* 'Zesy002' or 'Hort16A' plantlets, grown from axillary buds on Murashige and Skoog rooting medium without antibiotics in sterile 400-ml plastic tubs (pottles) with three plantlets per pottle, were purchased (Multiflora, Auckland, NZ). Plantlets were kept at 20°C under Gro-Lux fluorescent lights under long-day conditions (16 h light:8 h dark) and used when the plantlets were between 10 and 14 weeks old. Overnight liquid cultures of wild-type or mutant strains of *Psa* were pelleted at 6000 *g*, re-suspended in 500 ml of 10 mM $MgSO_4$ to an A_{600} = 0.05 ($\sim 5 \times 10^6$ CFU/ml, determined by plating). The surfactant Silwet™ L-77 (Lehle Seeds, Round Rock, USA) was added to the inoculum at 0.0025% (v/v) to facilitate leaf wetting. Pottles of 'Zesy002' or 'Hort16A' plantlets were filled with the inoculum, submerging the plantlets for 3 min, drained, sealed, and then incubated under previously described plant growth conditions. To assess *in planta* growth, leaf samples of four leaf discs per replicate, removed with a 1-cm diameter cork-borer, were taken at 2 h (day 0), day 6, and day 12 post-inoculation. All four pseudo-biological replicates per treatment were taken from the same pottle. To estimate *Psa* growth inside the plant, the leaf discs were surface sterilized, placed in Eppendorf tubes containing three sterile stainless-steel ball bearings and 350 µl 10 mM $MgSO_4$, and macerated in a Storm 24 Bullet Blender (Next Advance, NY, USA) for two bursts of 1 min each at maximum speed. A 10-fold dilution series of the leaf homogenates was made in sterile 10 mM $MgSO_4$ until a dilution of 10^{-8} and each dilution was plated as 10 µl droplets on LB agar supplemented with nitrofurantoin and cephalexin. After 2 days of incubation at 20°C, the CFU per cm^2 of leaf area was ascertained from dilutions. To observe disease symptoms on the plants, infected pottles were kept up to 50 days post-inoculation and photographs taken of whole pottles and a representative infected leaf. Infection severity was qualitatively assessed based on typical symptoms (in order of increasing severity): chlorotic haloes, necrotic leaf spots, leaf death, and plant death. Each of these growth assay experiments were conducted at least three times.

Hierarchical clustering and dendrogram analysis

Hierarchical cluster analysis was conducted in R (R-CoreTeam, 2018) using the ward.D2 method, as per the clustering analysis in the study by Baltrus *et al*. (2019). The 'phylogram' vignette was used to convert hierarchical clusters into dendrograms (Paradis and Schliep, 2018). The tanglegram function in the 'dendextend' package was used to visually compare dendrograms by connecting matching leaf node labels with lines (Galili, 2015). The ladder function was used to untangle dendrograms by rotating the tree branches at their nodes without altering their topology, allowing for clear visualization (Galili, 2015). The cor.dendlist function was used to calculate the cophenetic correlation coefficient for the compared dendrograms (Galili, 2015). Cophenetic correlation values (correlation coefficients) range from −1 to 1, with values close to 0 indicating that the compared dendrograms are not statistically similar. The resulting cophenetic correlation matrix was then visualized using the 'corrplot' package (Wei and Simko, 2017).

Acknowledgements

This work was funded (including a post-doctoral fellowship to J.J.) by the Bio-protection Research Centre (Tertiary Education Commission, New Zealand). L.M.H. would like to thank Zespri International for an MSc scholarship. The authors would like to thank Rick Broadhurst (AgResearch, Ruakura, New Zealand) for rabbit immunology. The authors would also like to thank Jo Bowen (PFR) and Iain Hay (UoA) for critically reading the manuscript.

References

Aziz, R.K., Bartels, D., Best, A.A., DeJongh, M., Disz, T., Edwards, R.A., *et al*. (2008) The RAST server: rapid annotations using subsystems technology. *BMC Genomics* **9**: 75.

Baltrus, D.A., Clark, M., Smith, C., and Hockett, K.L. (2019) Localized recombination drives diversification of killing spectra for phage-derived syringacins. *ISME J* **13**: 237–249.

Boratyn, G.M., Camacho, C., Cooper, P.S., Coulouris, G., Fong, A., Ma, N., *et al*. (2013) BLAST: a more efficient report with usability improvements. *Nucl Acids Res* **41**: W29–W33.

Butler, M.I., Stockwell, P.A., Black, M.A., Day, R.C., Lamont, I.L., and Poulter, R.T.M. (2013) *Pseudomonas syringae* pv. *actinidiae* from recent outbreaks of kiwifruit bacterial canker belong to different clones that originated in China. *PLoS One* **8**: e57464.

Carim, S., Azadeh, A.L., Kazakov, A.E., Price, M.N., Walian, P.J., Chakraborty, R., *et al*. (2020) Systematic discovery of pseudomonad genetic factors involved in sensitivity to tailocins. *bioRxiv* **2005**: 2027.113977.

Cunty, A., Poliakoff, F., Rivoal, C., Cesbron, S., Saux, M.L., Lemaire, C., *et al*. (2015) Characterization of *Pseudomonas syringae* pv. *actinidiae* (*Psa*) isolated from France and assignment of Psa biovar 4 to a *de novo* pathovar: *Pseudomonas syringae* pv. *actinidifoliorum* pv. Nov. *Plant Pathol* **64**: 582–596.

Cury, J., Jové, T., Touchon, M., Néron, B., and Rocha, E.P. C. (2016) Identification and analysis of integrons and cassette arrays in bacterial genomes. *Nucl Acids Res* **44**: 4539–4550.

Cuthbertson, L., Kimber, M.S., and Whitfield, C. (2007) Substrate binding by a bacterial ABC transporter involved in polysaccharide export. *Proc Natl Acad Sci* **104**: 19529–19534.

DebRoy, C., Fratamico, P.M., Yan, X., Baranzoni, G., Liu, Y., Needleman, D.S., *et al*. (2016) Comparison of O-antigen gene clusters of all O-serogroups of *Escherichia coli* and proposal for adopting a new nomenclature for O-typing. *PLoS ONE* **11**: e0147434.

Dillon, M.M., Almeida, R.N.D., Laflamme, B., Martel, A., Weir, B.S., Desveaux, D., and Guttman, D.S. (2019a) Molecular evolution of *Pseudomonas syringae* type III secreted effector proteins. *Front Plant Sci* **10**: 418.

Dillon, M.M., Thakur, S., Almeida, R.N.D., Wang, P.W., Weir, B.S., and Guttman, D.S. (2019b) Recombination of ecologically and evolutionarily significant loci maintains genetic cohesion in the *Pseudomonas syringae* species complex. *Genome Biol* **20**: 3.

Domingues, S., da Silva, G.J., and Nielsen, K.M. (2012) Integrons: vehicles and pathways for horizontal dissemination in bacteria. *Mobile Genet Elements* **2**: 211–223.

Engler, C., Gruetzner, R., Kandzia, R., and Marillonnet, S. (2009) Golden gate shuffling: a one-pot DNA shuffling method based on type iis restriction enzymes. *PLoS ONE* **4**: e5553.

Ey, P.L., Prowse, S.J., and Jenkin, C.R. (1978) Isolation of pure IgG1, IgG2a and IgG2b immunoglobulins from mouse serum using protein A-sepharose. *Immunochemistry* **15**: 429–436.

Frampton, R.A., Acedo, E.L., Young, V.L., Chen, D.N., Tong, B., Taylor, C., *et al*. (2015) Genome, proteome and structure of a T7-like bacteriophage of the kiwifruit canker phytopathogen *Pseudomonas syringae* pv. *actinidiae*. *Viruses* **7**: 3361–3379.

Frampton, R.A., Taylor, C., Moreno, A.V.H., Visnovsky, S.B., Petty, N.K., Pitman, A.R., and Fineran, P.C. (2014) Identification of bacteriophages for biocontrol of the kiwifruit canker phytopathogen *Pseudomonas syringae* pv. *actinidiae*. *Appl Environ Microbiol* **80**: 2216–2228.

Fujikawa, T., and Sawada, H. (2016) Genome analysis of the kiwifruit canker pathogen *Pseudomonas syringae* pv *actinidiae* biovar 5. *Sci Rep* **6**: 21399.

Galili, T. (2015) Dendextend: an R package for visualizing, adjusting and comparing trees of hierarchical clustering. *Bioinformatics* **31**: 3718–3720.

Ghequire, M.G.K., and De Mot, R. (2015) The tailocin tale: peeling off phage tails. *Trends Microbiol* **23**: 587–590.

Gillings, M.R. (2014) Integrons: past, present, and future. *Microbiol Mol Biol Rev* **78**: 257–277.

Hockett, K.L., Clark, M., Scott, S., and Baltrus, D.A. (2017) Conditionally redundant bacteriocin targeting by *Pseudomonas syringae*. *BioRxiv* **167**: 593.

Hockett, K.L., Renner, T., and Baltrus, D.A. (2015) Independent co-option of a tailed bacteriophage into a killing complex in *Pseudomonas*. *MBio* **6**: e00452.

Holtappels, D., Kerremans, A., Busschots, Y., Van Vaerenbergh, J., Maes, M., Lavigne, R., and Wagemans, J. (2020) Preparing for the KIL: receptor analysis of *Pseudomonas syringae* pv. *porri* phages and their impact on bacterial virulence. *Int J Mol Sci* **21**: 2930.

Jann, B., Reske, K., and Jann, K. (1975) Heterogeneity of lipopolysaccharides: analysis of polysaccharide chain lengths by sodium dodecylsulfate-polyacrylamide gel electrophoresis. *Eur J Biochem* **60**: 239–246.

Kandel, P.P., Baltrus, D.A., and Hockett, K.L. (2020) *Pseudomonas* can survive tailocin killing via persistence-like and heterogenous resistance mechanisms. *J Bacteriol* **202**: JB.00142-00120.

King, J.D., Kocincova, D., Westman, E.L., and Lam, J.S. (2009) Review: lipopolysaccharide biosynthesis in *Pseudomonas aeruginosa*. *Innate Immun* **15**: 261–312.

Koh, Y., Cha, B., Chung, H., and Lee, D. (1994) Outbreak and spread of bacterial canker in kiwifruit. *Korean J Plant Pathol* **10**: 68–72.

Kutschera, A., Schombel, U., Wröbel, M., Gisch, N., and Ranf, S. (2019a) Loss of *wbpL* disrupts O-polysaccharide synthesis and impairs virulence of plant-associated *Pseudomonas* strains. *Mol Plant Pathol* **20**: 1535–1549.

Kutschera, A., Dawid, C., Gisch, N., Schmid, C., Raasch, L., Gerster, T., *et al*. (2019b) Bacterial medium-chain 3-hydroxy fatty acid metabolites trigger immunity in *Arabidopsis* plants. *Science* **364**: 178–181.

Kvitko, B.H., and Collmer, A. (2011) Construction of *Pseudomonas syringae* pv. *tomato* DC3000 mutant and polymutant strains. In *Plant Immunity: Methods and Protocols*, McDowell, J.M. (ed). Totowa, NJ: Humana Press, pp. 109–128.

Lam, J., Taylor, V., Islam, S., Hao, Y., and Kocíncová, D. (2011) Genetic and functional diversity of *Pseudomonas aeruginosa* lipopolysaccharide. *Front Microbiol* **2**: 118.

Lerouge, I., and Vanderleyden, J. (2002) O-antigen structural variation: mechanisms and possible roles in animal/plant–microbe interactions. *FEMS Microbiol Rev* **26**: 17–47.

Liston, S.D., Clarke, B.R., Greenfield, L.K., Richards, M.R., Lowary, T.L., and Whitfield, C. (2015) Domain interactions control complex formation and polymerase specificity in the biosynthesis of the *Escherichia coli* O9a antigen. *J Biol Chem* **290**: 1075–1085.

Maier, R.J., and Brill, W.J. (1978) Involvement of *Rhizobium japonicum* O antigen in soybean nodulation. *J Bacteriol* **133**: 1295–1299.

Maldonado, R.F., Sá-Correia, I., and Valvano, M.A. (2016) Lipopolysaccharide modification in gram-negative bacteria during chronic infection. *FEMS Microbiol Rev* **40**: 480–493.

Mann, E., Kelly, S.D., Al-Abdul-Wahid, M.S., Clarke, B.R., Ovchinnikova, O.G., Liu, B., and Whitfield, C. (2019) Substrate recognition by a carbohydrate-binding module in the prototypical ABC transporter for lipopolysaccharide O antigen from *Escherichia coli* O9a. *J Biol Chem* **294**: 14978–14990.

Marcelletti, S., Ferrante, P., Petriccione, M., Firrao, G., and Scortichini, M. (2011) *Pseudomonas syringae* pv. *actinidiae* draft genomes comparison reveal strain-specific features involved in adaptation and virulence to *Actinidia* species. *PLoS ONE* **6**: 17.

Mazzaglia, A., Studholme, D.J., Taratufolo, M.C., Cai, R.M., Almeida, N.F., Goodman, T., *et al*. (2012) *Pseudomonas syringae* pv. *actinidiae* (Psa) isolates from recent bacterial canker of kiwifruit outbreaks belong to the same genetic lineage. *PLoS ONE* **7**: 11.

McAtee, P.A., Brian, L., Curran, B., van der Linden, O., Nieuwenhuizen, N.J., Chen, X., *et al*. (2018) Reprogramming of *Pseudomonas syringae* pv. *actinidiae* gene expression during early stages of infection of kiwifruit. *BMC Genomics* **19**: 822.

McCann, H.C., Li, L., Liu, Y., Li, D., Hui, P., Zhong, C., *et al*. (2017) The origin and evolution of a pandemic lineage of the kiwifruit pathogen *Pseudomonas syringae* pv *actinidiae*. *Genome Biol Evol* **9**: 932–944.

McCann, H.C., Rikkerink, E.H.A., Bertels, F., Fiers, M., Lu, A., Rees-George, J., *et al*. (2013) Genomic analysis of the kiwifruit pathogen *Pseudomonas syringae* pv. *actinidiae* provides insight into the origins of an emergent plant disease. *PLoS Pathog* **9**: e1003503.

Mesarich, C.H., Rees-George, J., Gardner, P.P., Ghomi, F. A., Gerth, M.L., Andersen, M.T., *et al*. (2017) Transposon insertion libraries for the characterization of mutants from the kiwifruit pathogen *Pseudomonas syringae* pv *actinidiae*. *PLoS ONE* **12**: e0172790.

Ovod, V., Rudolph, K., and Krohn, K. (1997a) Demonstration of the immunological diversity of O-chains of lipopolysaccharide of *Pseudomonas syringae* and inferring of the serogroup- and serotype-specific epitopes with monoclonal antibodies. In *Pseudomonas Syringae Pathovars and Related Pathogens*, Rudolph, K., Burr, T.J., Mansfield, J. W., Stead, D., Vivian, A., and von Kietzell, J. (eds). Dordrecht: Springer, pp. 532–537.

Ovod, V., Rudolph, K., and Krohn, K. (1997b) Serological classification of *Pseudomonas syringae* pathovars based on monoclonal antibodies towards the lipopolysaccharide-O-chains. In *Pseudomonas Syringae Pathovars and Related Pathogens*, Rudolph, K., Burr, T.J., Mansfield, J. W., Stead, D., Vivian, A., and von Kietzell, J. (eds). Dordrecht: Springer, pp. 526–531.

Paradis, E., and Schliep, K. (2018) Ape 5.0: an environment for modern phylogenetics and evolutionary analyses in R. *Bioinformatics* **35**: 526–528.

Pinheiro, L.A.M., Pereira, C., Frazão, C., Balcão, V.M., and Almeida, A. (2019) Efficiency of phage φ6 for biocontrol of *Pseudomonas syringae* pv. *syringae*: an *in vitro* preliminary study. *Microorganisms* **7**: 286.

R-CoreTeam. (2018) *R: A Language and Environment for Statistical Computing*. Vienna: R Foundation for Statistical Computing. https://www.R-project.org.

Raetz, C.R., and Whitfield, C. (2002) Lipopolysaccharide endotoxins. *Annu Rev Biochem* **71**: 635–700.

Riley, M.A., and Wertz, J.E. (2002) Bacteriocins: evolution, ecology, and application. *Annu Rev Microbiol* **56**: 117–137.

Rooney, W.M., Grinter, R.W., Correia, A., Parkhill, J., Walker, D.C., and Milner, J.J. (2020) Engineering bacteriocin-mediated resistance against the plant pathogen *Pseudomonas syringae*. *Plant Biotechnol J* **18**(5): 1296–1306.

Sambrook, J., and Russell, D.W. (2001) *Molecular Cloning: A Laboratory Manual*, 3rd ed. New York, NY: Cold Spring Harbour.

Sawada, H., Kondo, K., and Nakaune, R. (2016) Novel biovar (biovar 6) of *Pseudomonas syringae* pv. *actinidiae* causing bacterial canker of kiwifruit (*Actinidia deliciosa*) in Japan. *Jpn J Phytopathol* **82**: 101–115.

Schafer, A., Tauch, A., Jager, W., Kalinowski, J., Thierbach, G., and Puhler, A. (1994) Small mobilizable multipurpose cloning vectors derived from the *Escherichia coli* plasmids pk18 and pk19 - selection of defined deletions in the chromosome of *Corynebacterium glutamicum*. *Gene* **145**: 69–73.

Scortichini, M., Marcelletti, S., Ferrante, P., Petriccione, M., and Firrao, G. (2012) *Pseudomonas syringae* pv. *actinidiae*: a re-emerging, multi-faceted, pandemic pathogen. *Mol Plant Pathol* **13**: 631–640.

Serizawa, S., Ichikawa, T., Takikawa, Y., Tsuyumu, S., and Goto, M. (1989) Occurrence of bacterial canker of kiwifruit in Japan description of symptoms, isolation of the pathogen and screening of bactericides. *Jpn J Phytopathol* **55**: 427–436.

Takikawa, Y., Serizawa, S., Ichikawa, T., Tsuyumu, S., and Goto, M. (1989) *Pseudomonas syringae* pv. *actinidiae* pv. Nov the causal bacterium of canker of kiwifruit in Japan. *Jpn J Phytopathol* **55**: 437–444.

Vanneste, J.L., Yu, J., Cornish, D.A., Tanner, D.J., Windner, R., Chapman, J.R., *et al*. (2013) Identification, virulence, and distribution of two biovars of *Pseudomonas syringae* pv. *actinidiae* in New Zealand. *Plant Dis* **97**: 708–719.

Wei, T. and Simko, V. (2017) R package 'corrplot': visualization of a correlation matrix (version 0.84) https://github.com/taiyun/corrplot.

Westphal, O., and Jann, K. (1965) Bacterial lipopolysaccharide: extraction with phenol-water and further application of the procedure. *Meth Carbohydr Chem* **5**: 83–91.

Wyres, K.L., Gorrie, C., Edwards, D.J., Wertheim, H.F.L., Hsu, L.Y., Van Kinh, N., *et al*. (2015) Extensive capsule locus variation and large-scale genomic recombination within the *Klebsiella pneumoniae* clonal group 258. *Genome Biol Evol* **7**: 1267–1279.

Zdorovenko, E.L., Ovod, V.V., Zatonsky, G.V., Shashkov, A. S., Kocharova, N.A., and Knirel, Y.A. (2001) Location of the O-methyl groups in the O-polysaccharide of *Pseudomonas syringae* pv. *phaseolicola*. *Carbohydr Res* **330**: 505–510.

Zdorovenko, G.M., and Zdorovenko, E.L. (2010) *Pseudomonas syringae* lipopolysaccharides: immunochemical characteristics and structure as a basis for strain classification. *Microbiology* **79**: 47–57.

Supporting Information

Additional Supporting Information may be found in the online version of this article at the publisher's web-site:

Fig. S1. MLST genome phylogenetic tree for *Pseudomonas syringae* and *Pseudomonas viridiflava* strains. Five genes (*gyrB*, *ropD*, *gapA*, *pgi* and *acnB*) from selected representatives of *P. syringae* phylogroups were concatenated and aligned in Geneious v11 and neighbour-joining phylogenetic trees built. Strains grouped as expected into their phylogroups and are coloured according to their core genome phylogenies as previously described (Dillon *et al*., 2019b): phylogroup 1 blue; phylogroup 2 red; phylogroup 3 green; phylogroup 4 orange; phylogroup 5 purple; phylogroup 6 yellow; phylogroup 7 pink; phylogroup 9 grey; phylogroup 10 mauve; phylogroup 11 chocolate; phylogroup 13 claret.

Fig. S2. Schematic for knock-out and knock-in swap of the TET locus in *Pseudomonas syringae* pv. *actinidiae* (*Psa*) BV1. One-kilobase flanking regions upstream (UP) and downstream (DN) of the polymorphic region of the TET operon in wild-type (WT) *Psa* BV1 (green; encoding Wzt, WbdD, and WbdA proteins in red) were PCR-cloned and fused at a primer-introduced internal *Xba*I site and used in pK18mobsacB vector-mediated knock-out of the BV1 TET locus to generate BV1_LPS-KO. To generate the BV1-to-BV3 LPS swap (knock-in complementation), a pK18mobsacB vector-mediated method was also used. First, *Eco53k*I, *Bsa*I and *Pst*I sites were removed during PCR (primer-driven) to facilitate blunt-end cloning of modules, golden gate (GG) cloning, and evasion of the BV1-encoded restriction enzyme, respectively. The knock-in pK18mobsacB vector was built (GG assembly) from five modules with sizes indicated. Modules 2, 3, and 5 were PCR-amplified and blunt-end cloned into pICH41021 shuttle vector directly. Modules 1 and 4 were first cloned as two parts (A and B) from their respective *Psa* BVs and then fused by overlap PCR mediated by primer sequences designed to introduce overlap regions during amplification of part A and B. Following overlap PCR, modules 1 and 4 were blunt-end cloned into the pICH41021 shuttle vector. The modules were then assembled into the final pK18mobsacB knock-in construct. The BV1_LPS-KO was then subsequently complemented with TET operon from BV3 (blue).

Fig. S3. Bacterial cell sedimentation for *Pseudomonas syringae* pv. *actinidiae* (*Psa*) in inoculation buffer. (A) *Psa* BV3 and two R-LPS mutants, Δ*wbpL* and Δ*gmd* (Mesarich *et al*., 2017) were grown overnight in LB liquid culture, pelleted by centrifugation, resuspended in 10 mM $MgSO_4$ buffer, and normalized to OD_{600} of 0.4. (B) *Psa* BV3 and BV1 (wild-type; WT), *Psa* BV1 LPS knock-out (Δ*LPS*), four BV1-to-BV3 TET operon-complemented knock-in isolates (Δ*LPS* + *LPS_BV3* #1–2, #1–4, #2–1, and #2–5; green), and four BV1 revertant to knock-out isolates (Δ*LPS-LPSrev*: #1–3, #1–6, #2–4, and #2–8; red) were grown overnight in LB liquid culture, pelleted by centrifugation, resuspended in 10 mM $MgSO_4$ buffer, and normalized to OD_{600} of 0.5. Photographs of cell suspensions in both (A) and (B) were taken immediately after resuspension in buffer (T0) and after an hour standing at room temperature (T1).

Fig. S4. Colony morphologies for *Pseudomonas syringae* pv. *actinidiae* (*Psa*) BV1 mutant and complemented strains. *Psa* BV3 mutants (Δ*wbpL* or Δ*gmd*) (Mesarich *et al*., 2017) and BV1 (wild-type; WT), *Psa* BV1 LPS knock-out (Δ*LPS*), four BV1-to-BV3 TET operon complemented knock-in isolates (Δ*LPS* + *LPS_BV3* #1–2, #1–4, #2–1, and #2–5; green), and four BV1 revertant to knock-out isolates (Δ*LPS-LPSrev*: #1–3, #1–6, #2–4, and #2–8; red) were grown on LB agar plates, for 3 days and photographs of colonies were taken under a stereomicroscope.

Fig. S5. The CPA TET operon is required for symptom development of *Pseudomonas syringae* pv. *actinidiae* (*Psa*) in host plants. (A) *P*sa BV3 or BV3 R-LPS mutants (Mesarich *et al*., 2017) were flood-inoculated at $\sim 10^6$ CFU/ml on *Actinidia chinensis* var. *chinensis* 'Zesy002', and photographs of symptom development in pottles and representative leaves taken at 50 days post-inoculation. (B) *P*sa BV1, BV1 LPS knock-out mutant (Δ*LPS*), or two independent BV1 knock-outs complemented LPS from BV3 (+*LPS_BV3*) mutants were flood-inoculated at $\sim 10^6$ CFU/ml on *A. chinensis* var. *chinensis* 'Hort16A', and photographs of symptom development in pottles and representative leaves taken at 50 days post-inoculation. Lesions are indicated by white arrows.

Fig. S6. Comparative schematic of the CPA locus from isolates of *P. syringae*. Isolates chosen to illustrate the variation at this locus were *Psa* BV1 ICMP 9853, *Psy* B728a, *Psa* BV3 ICMP 18884. *Ps* ICMP 11168, *Ps* ICMP 19499, *Pto* DC3000, *Pta* ICMP 2835 and *Ps* ICMP 19198. From the left tRNA-Met (red) and genes encoding DnaJ and a methylchemotactic receptor (grey) are found in all isolates. Genes encoding D-Rha and L-Rha are coloured dark and light blue respectively. Genes encoding the TET operon are various shades of green reflecting the different versions of this locus in each isolate. Note the fusion of the last two

genes of this operon in isolates *Ps* ICMP 19499, *Pto* DC3000, *Pta* ICMP 2835 and *Ps* ICMP 19198. Genes that have not been functionally identified but are likely to have a role in CPA biosynthesis are coloured orange.

Fig. S7. Cophenetic entanglement coefficients for phylogenetic trees for the TET operon and MLST analysis generated using different tree-building methods (UPGMA, Neighbour joining (NJ), or RAxML) compared to each other and to the R-syringacin (tailocin) sensitivity tree for data from Baltrus *et al*. (2019). The cophenetic correlation matrix between the trees have values ranging between −1 to 1, with near 0 values indicating that the two trees are not statistically similar. Values between −0.25 and 0.25 (indicated by the red box on the scale) are poorly correlated and outlined in the table and associated scale. UPGMA was selected over RAxML and NJ for tree-building in Fig. 6 due to the nature of comparing the sensitivity phenotype with genetic similarity treated as a 'phenotype' (thus creating phenetic trees rather than phylogenetic trees). This allowed for pairwise comparisons instead of inferring an evolutionary relationship that NJ and RAxML trees are better at conveying.

Table S1. Metadata for isolates used in this study

Table S2. The sequence of primers used in this study. All primers were synthesized by Macrogen, South Korea.